Published in final edited form as:

Cell Rep. 2016 November 1; 17(6): 1505–1517. doi:10.1016/j.celrep.2016.10.018.

Role for the IFT-A complex in selective transport to the primary cilium

Wenxiang Fu[1], **Lei Wang**[1], **Sehyun Kim**[1,#], **Ji Li**[2], and **Brian David Dynlacht**[1,*]

[1]Department of Pathology and Perlmutter Cancer Center, NYU School of Medicine, Smilow Research Building, 522 First Avenue, New York, NY 10016

[2]Department of Medical Oncology, Dana-Farber Cancer Institute, Harvard Medical School, Boston, MA, 02115; Broad Institute, Cambridge, MA 02142

Summary

Intraflagellar transport sub-complex A (IFT-A) is known to regulate retrograde IFT in the cilium. To rigorously assess its other possible roles, we knocked out an IFT-A subunit, *IFT121*/*WDR35*, in mammalian cells and screened the localization of more than 50 proteins. We found that Wdr35 regulates cilium assembly by selectively regulating transport of distinct cargoes. Beyond its role in retrograde transport, we show that Wdr35 functions in fusion of Rab8 vesicles at the nascent cilium, protein exit from the cilium, and centriolar satellite organization. Further, we show that Wdr35 is essential for entry of many membrane proteins into the cilium through robust interactions with cargoes and other IFT-A subunits, but the actin network functions to dampen this transport. Wdr35 is mutated in several ciliopathies, and we find that certain disease mutations impair interactions with cargo and other IFT-A subunits. Together, our data link defects in IFT-A mediated cargo transport with disease.

eTOC Blurb

Fu et al. find that Wdr35-containing intraflagellar transport sub-complex A (IFT-A) regulates selective transport of distinct cargoes for primary cilium assembly. Wdr35 is essential for entry of many membrane proteins into the cilium.

*Correspondence: Brian.Dynlacht@nyumc.org.
#Current address: Genentech, Inc., 1 DNA Way, South San Francisco, CA 94080

Author contributions

W.F. and B.D.D. conceived the project, designed research and analyzed data. W.F. and L.W. discussed the CRISPR design, S.K., W.F. and L.W. performed the EM study, J.L. performed preliminary experiments using Wdr35 cDNAs and siRNAs, W.F. performed all other experiments, W.F. and B.D.D. wrote the paper, and all authors participated in the discussion of the data and production of the final version of the manuscript.

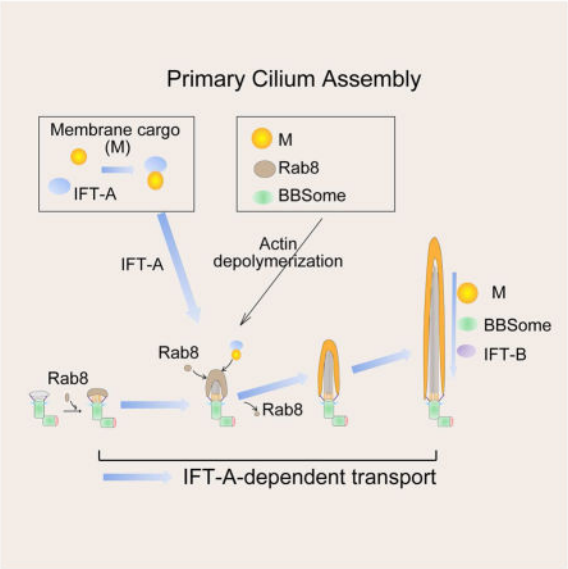

Introduction

The primary cilium, an antenna-like structure protruding from the cell surface, is essential for multiple signaling pathways and development (Fu et al., 2014; Nozawa et al., 2013). The primary cilium is derived from centrosomes and is maintained by intraflagellar transport (IFT) particles, including two protein sub-complexes, IFT-A and IFT-B (Engel et al., 2012; Hao and Scholey, 2009). IFT-B and IFT-A were shown to regulate anterograde and retrograde IFT within the cilium, respectively (Bhogaraju et al., 2013b; Ocbina et al., 2011; Tran et al., 2008). Tubulin and outer dynein arm components were found to be cargoes of IFT (Ahmed et al., 2008; Bhogaraju et al., 2013a; Hou et al., 2007). However, other IFT cargoes, especially those conveyed by IFT-A, remain largely undefined (Lechtreck, 2015; Liem et al., 2012; Mukhopadhyay et al., 2010). IFT121/Wdr35, which assembles into the IFT-A complex with five other subunits (IFT144/Wdr19, IFT140, IFT139/Ttc21b, IFT122, and IFT43) (Cole and Snell, 2009), was shown to be required for retrograde IFT in *C. elegans* (Blacque et al., 2006). In *WDR35* null MEFs, retrograde transport of IFT88 within cilia is disrupted (Mill et al., 2011), and a previous report, published while our work was in progress, showed that the membrane proteins, Evc1/2 and Smo, did not localize to cilia (Caparros-Martin et al., 2015). Further, knock-down of Wdr35 in RPE1 cells led to variable effects on cilium targeting of two G protein-coupled receptors (GPCRs) (Mukhopadhyay et al., 2010). Moreover, experiments performed with mouse *IFT144* mutants suggested that this IFT-A subunit is required for proper cilium assembly, likely as a result of roles in both retrograde and anterograde transport (Liem et al., 2012). However, mechanistic links between the IFT-A complex and transport to the cilium or anterograde transport have not been previously explored.

Mutations in *WDR35* and other IFT-A subunits have been found in patients with ciliopathies (Alazami et al., 2014; Gilissen et al., 2010; Mill et al., 2011; Perrault et al., 2012), such as short-rib polydactyly and Sensenbrenner syndrome/cranioectodermal dysplasia (CED) with

ectodermal and skeletal abnormalities. However, it is not known how different disease-related *WDR35* mutations affect its function, and the relationship between *WDR35* mutations and ciliopathies is largely unknown. Here, we have comprehensively examined the impact of knocking out *WDR35* in human RPE1 cells. By examining the localization of a large set of centrosome- and cilium-related proteins in *WDR35* knockout (KO) cells, we suggest that Wdr35 plays key roles in cargo transport in concert with other IFT-A subunits. Further, the collaboration of Wdr35-dependent cargo transport and the actin network, as well as the link between cargo transport defects and disease, reveal the potential for therapeutically targeting diseases associated with IFT-A mutations.

Results

Wdr35 loss results in multiple defects, including abnormal transport within, and exit from, the cilium

To better understand Wdr35 function, we knocked out the *WDR35* gene using CRISPR/Cas9 (Cong et al., 2013; Haurwitz et al., 2010) in human RPE1 cells (Figure S1A). We obtained *WDR35* knock-out (KO) clones, #1 and #2, using two different single guide RNAs (sgRNAs) targeting exons 1 and 2 of *WDR35* (Figure S1A). Sequencing of both clones identified insertion/deletions in the genomic locus, which are expected to lead to premature termination of WDR35 translation. We detected Wdr35 expression using quantitative reverse transcription-coupled PCR (qRT-PCR). The sizes and levels of cDNA amplicons using different primers confirmed the edited genomes in the two *WDR35* KO clones. Wdr35 mRNA in clone #2 was markedly decreased, probably as a result of nonsense-mediated mRNA decay (Lykke-Andersen and Jensen, 2015). As described below, we showed that defects in ciliogenesis were rescued by full-length Wdr35, confirming that none of the resulting phenotypes arose from off-target mutations (Figures 6A–6D). Moreover, western blotting of lysates showed that expression of several centrosomal and ciliary proteins was not altered in the *WDR35* KO (Figure S1*B*).

First, we examined the assembly and structure of primary cilia in *WDR35* KO cells by transmission electron microscopy (TEM) after 48 h of serum starvation (SS). Our analysis revealed that Wdr35 is required for normal cilium structure (Figure 1A), consistent with phenotypes observed in mice carrying null alleles of IFT-A components(Liem et al., 2012; Ocbina et al., 2011; Qin et al., 2011). Thus, we found that cilia in *WDR35* KO cells are shorter and bulbous, exhibiting abnormal morphology of both the axoneme and ciliary membrane, as well as an aberrant distribution of electron-dense particles. A comparison of ciliation frequency at early and later time points indicated that *WDR35* ablation led to both decreases and delays in cilium assembly (Figures 1B, 1C, S1C and S1D). In contrast with the slight reduction of IFT88-positive cilia after *WDR35* ablation, there was a strong reduction in the occurrence of cilia positive for modified tubulin markers, namely, glutamylated (GT335+), acetylated (Ace-tub+), and detyrosinated (Detyro-tub+) tubulin. To comprehensively explore the roles of Wdr35 at the centrosome and cilium, we examined the localization of >50 proteins before and after ciliation (Table S1) in *WDR35* KO cells. We found that many components, including distal appendage proteins and transition zone markers, were not affected in the *WDR35* KO (Figure S1C-S1F). Likewise, attachment and

morphology of early ciliary vesicles that dock to the distal appendage were not affected (Figure 1D).

Next, we examined Rab8 (Figure 1E), which localizes to developing cilia (Kobayashi et al., 2014; Lu et al., 2015; Westlake et al., 2011). Rab8 first appears at centrioles as puncta that extend through subsequent fusion events to form tube-like structures. Interestingly, the tube-like Rab8 staining was dramatically reduced in *WDR35* KO cells, although the total number of cells with Rab8-positive foci was less strongly affected. Further, the localization of several other vesicle–associated proteins, including Rab11, was not affected, and Golgi morphology and endocytic transferrin uptake were not impacted by *Wdr35* ablation, ruling out other vesicular functions for Wdr35 (Figure S1C). Together, these findings indicate that Wdr35 is required for growth of Rab8 vesicles after initial docking during cilia assembly.

In agreement with the role of IFT-A in retrograde transport, the *WDR35* KO exhibited defects in retrograde transport and exit of IFT88 from the cilium (Figures 1F, S1C and S2A). In cells lacking Wdr35, IFT88 forms a ‘bulb’ within the cilium characterized by its aberrant accumulation, primarily at the tip. Wdr35 also regulated the retrograde transport of many proteins with diverse functions, including other IFT-B subunits (IFT54 and IFT20), anterograde IFT motor Kif3A, IFT-A subunits (IFT140 and IFT144), BBsome subunits (BBS4 and BBS5), and the Hedgehog (Hh) pathway-associated transcription factor, Gli2 (Figures 1F–1H and S2B–S2F). Because the BBSome is normally rapidly exported from cilia in mammalian cells (Eguether et al., 2014; Liew et al., 2014), the markedly increased percentages of BBS4- and BBS5-positive cilia in *WDR35* KO cells indicated defective ciliary exit stemming from aberrant retrograde transport (Figure 1H).

Wdr35 null cells exhibit marked defects in cargo transport to the cilium

Importantly, we observed severe ciliary import defects in *WDR35* KO cells. First, we noted defective entry of the IFT-A component, IFT144, into cilia, suggesting that interactions with Wdr35 were essential (Figure S2D), in contrast with the relatively minor impact on IFT88 (IFT-B) import (Figure 1F). Second, we found that Wdr35 was required for Arl13b cilium entry using two different antibodies and exogenously expressed GFP-tagged Arl13b (Figures 2A, S2G and S2H). Strikingly, Arl13b was not observed in cilia of *WDR35* KO cells serum starved for different durations (Figure 2B). We found that in control RPE1 cells, although most cilia were positive for both IFT88 and Arl13b, a small percentage of cilia showed strong localization of either IFT88 or Arl13b (Figure 2C), suggesting that cells might use alternative pathways for cilium entry of IFT-B and membrane proteins. Another membrane protein, INPP5E, was also excluded from cilia after Wdr35 ablation (Figures 2A, 2D and S2G). Likewise, ciliary entry of three G protein-coupled receptors (GPCRs; serotonin receptor ($5HT_6$), MCHR1, and SSTR3) was dependent on Wdr35 (Figures 2E–2G and S2I). The localization of Smoothened (Smo) is dependent on Hedgehog activation(Corbit et al., 2005), but even in the presence of a Hedgehog agonist, SAG, Smo was not efficiently targeted to cilia in *WDR35* KO cells (Figures 2H and 2I), similar to results obtained with null *Wdr35* MEFs (Caparros-Martin et al., 2015). A mild defect in retrograde transport of Smo was also observed in *WDR35* KO cells (Figure 2I). Interestingly, unlike endogenous Smo, ectopically expressed GFP-Smo localized to cilia without hedgehog stimulation

(Kovacs et al., 2008), and in *WDR35* KO cells expressing this fusion protein, retrograde transport defects were primarily observed (Figures 2J and S2J), suggesting that cilium entry of GFP-Smo in the absence of Wdr35 relies on a Wdr35-independent pathway, perhaps involving β arrestin-mediated targeting (Kovacs et al., 2008). Like Smo, Arl13b and INPP5E also displayed retrograde transport defects in the small percentage (<10%) of *WDR35* KO cells able to import these proteins into the cilium (Figure 2K).

To test whether the role of Wdr35 in cargo transport was restricted to RPE1 cells, we also generated *WDR35* KO 293T cells (Figure S2K). We found that Wdr35 was also required for retrograde intraflagellar transport of IFT88 and ciliary entry of Arl13b in these cells (Figures S2L–S2O), suggesting functional conservation of Wdr35 in both cell lines. We examined whether ciliary import coincided with stable interactions with Wdr35. Immunoprecipitation (IP) of 293T cell extracts showed that Wdr35 bound to Arl13b but not IFT88 or Cep41 (Figure 2L), suggesting stable interactions with select proteins most dramatically affected by Wdr35 loss. Together, these findings indicate that Wdr35 is essential for transporting a subset of protein cargoes into the cilium, and once inside the cilium, several proteins are continuously transported by Wdr35-dependent retrograde IFT. Because Wdr35 promotes targeting of Arl13b, INPP5E and Rab8 during early ciliogenesis, when the nascent ciliary vesicle has not fused with the cell membrane, we conclude that Wdr35 plays an important role in regulating transport of these proteins directly from the cytoplasm.

Integrated function of Wdr35-IFT-A complex

To investigate whether Wdr35 functions independently or in concert with the IFT-A complex to transport cargoes, we knocked down IFT43 and IFT144 in RPE1 cells and examined the localization of three cargoes (IFT88, BBS4, and Arl13b) (Figures 3A–3D, S3A and S3B). Our data indicate that, like the *WDR35* KO, knock-down of Wdr35, IFT43, or IFT144 led to defects in retrograde transport of IFT88 and BBS4 and abolished entry of Arl13b into the cilium. The consistent roles of Wdr35, IFT43, and IFT144 suggest that the IFT-A complex acts in concert to transport these cargoes.

To understand how Wdr35 collaborates with other IFT-A proteins, we performed an extensive series of immunoprecipitations (Figures 3E–3G and S3C–S3M) on four IFT-A subunits (Wdr35, IFT43, IFT122, and IFT139) and three ciliary membrane cargoes (Arl13b, SSTR3, and INPP5E) using extracts of growing and quiescent RPE1 cells as well as proliferating 293T cells. We found that interactions among these seven proteins form a network (Figure 3H). Most importantly, ciliary membrane proteins interacted with each of these IFT-A subunits, supporting the conclusion that Wdr35 assembles an integrated IFT-A complex competent for transport of cargo. Robust interactions among these proteins could be detected in growth medium with serum, where levels of ciliation are low. This finding reinforces the observation that the interaction of IFT-A components and membrane cargoes can occur outside of cilia. Of note, the expression of exogenous wdr35 and IFT122 was much lower after serum-starvation (Figures S3C and S3D), and their interactions were, correspondingly, more weakly detected.

Arl13b-INPP5E and Arl13b-SSTR3 interactions were also observed, suggesting coordinated transport of diverse cargoes. Indeed, INPP5E was also found to be targeted to cilia by

Arl13b and PDE6D (Humbert et al., 2012; Thomas et al., 2014), consistent with the coincident loss of localization of multiple membrane proteins after ablation of Wdr35. It has been shown that Arl13b interacts with IFT-B components via IFT46 and IFT74 (Cevik et al., 2013), and our data suggest the existence of a separate Arl13b-IFT-A complex independent of IFT-B.

Role for Wdr35 in centriolar satellite assembly

During our search for possible Wdr35-regulated targets, we found that the relative intensity of four centriolar satellite proteins (Cep290, PCM1, Cep131 and BBS4) was reduced in the proximity of centrosomes after *WDR35* ablation (Figures S4A and S4B). However, the overall abundance of PCM1 and Cep290 was not impacted by Wdr35 loss (Figure S1B), suggesting that these proteins were aberrantly localized in the absence of Wdr35. Likewise, depletion of IFT43, IFT144, or Wdr35 with siRNAs led to similar reductions in centriolar satellite proteins around centrosomes (Figures S3A and S4C-S4F). Satellite dispersal after IFT-A knock-down was less dramatic when compared with PCM1 knock-down, consistent with the notion that IFT-A proteins are not core components of centriolar satellites. GFP-Wdr35 partially co-localized with PCM1 and Cep290 (Figure S4G), and Wdr35 was able to bind Cep290 (Figure S6C). Together these results indicate that Wdr35 and other IFT-A subunits are required for proper centriolar satellite organization. Given that BBS4, a ciliary cargo of Wdr35, is also involved in satellite organization (Kim et al., 2004), and several centriolar satellite proteins function in cilia assembly (Kim et al., 2008; Tsang et al., 2008), Wdr35-dependent centriolar satellite organization could be linked with its roles at cilia.

A role for the actin network in the regulation of WDR35 function

Actin polymerization antagonizes ciliogenesis, whereas de-polymerization by Cytochalasin D (CytoD) promotes cilium assembly and elongation of cilia (Cao et al., 2012; Kim et al., 2015; Kim et al., 2010). We tested a connection between Wdr35 function and actin by perturbing the actin network with CytoD. As expected, the global filamentous actin (F-actin) network was significantly disrupted by CytoD treatment (Figure S5A). Strikingly, examination of multiple cilia markers (GT335, Arl13b, IFT54, IFT88, BBS5, INPP5E and Rab8) revealed functional interactions between Wdr35-dependent transport and the actin network (Figures 4A, S5B and S5C). First, in *WDR35* KO cells, CytoD treatment partially rescued the occurrence of GT335-positive cilia and the “bulb-like” accumulation of IFT88, IFT54, and BBS5 (Figures 4A–D). CytoD treatment also increased the percentages of acetylated tubulin (Ace-tub+) and detyrosinated tubulin-positive (Detyro-tub+) cilia, although tubulin modifications in the cytoplasm were not affected by actin destabilization (Figures S5D–S5G). Unlike the control, elongated cilia were not consistently observed after CytoD treatment of *WDR35* KO cells, and IFT54 and BBS5 exit from the cilium was not rescued (Figures 4A and 4E–4G). As noted, cilia in *WDR35* KO cells were enriched with IFT-B and the BBSome but lacked Arl13b and INPP5E owing to defects in both retrograde IFT and ciliary entry (Figures 1 and 2). Remarkably, we found that CytoD treatment substantially rescued the defects in Arl13b and INPP5E entry provoked by *WDR35* ablation (Figures 4A, 4H–4J, S5B and S5C). Interestingly, CytoD treatment, which increases cilium targeting of BBS5 (Figure 1G), also dramatically increased Rab8 recruitment to cilia in both control and *WDR35* KO cells (Figures 4A and 4K). Due to its departure from mature cilia

(Westlake et al., 2011), Rab8 tends to concentrate at proximal ciliary regions, whereas CytoD promoted its accumulation at distal regions, similar to the pattern of Rab8 in elongating cilia. Thus, as a result of the combined rescue of protein ciliary targeting and partial restoration of retrograde transport, cilia in CytoD-treated *WDR35* KO cells were enriched for Arl13b, INPP5E, Rab8, IFT-B, and BBSome as compared to the untreated KO cells (Figure S6J). We also found that the bulbous accumulation of IFT-B was partially alleviated by CytoD treatment, perhaps as a result of enhanced cilium-targeting of membrane proteins such as Arl13b, which associates with IFT-B (Cevik et al., 2013), and subsequent diffusion or transport (Li et al., 2010). Further, we treated cells with LiCl, which also leads to cilium elongation in control cells, possibly by promoting tubulin acetylation (Ahmed et al., 2008), but unlike CytoD treatment, it neither increased Arl13b entry nor diminished the IFT54 'bulb' in *WDR35* KO cells (Figure S5H). These results suggested that rescue of transport phenotypes observed in *WDR35* KO cells was not simply a consequence of restoring cilium length.

These findings prompted us to further explore the connections between the actin network and Arl13b transport. We found that the bulk of cytoplasmic foci of Arl13b were associated with actin in RPE1 cells, and their co-localization was most apparent at the leading edge (Figures 4L and S5I). As visualized by phalloidin-FITC (Figure 4L), CytoD treatment dramatically depolymerized actin filaments, promoting formation of numerous actin "nodes" as described in cells treated with another actin depolymerization drug, Latrunculin A (Luo et al., 2013). We found that in contrast with the association of Arl13b with actin filaments in vehicle-treated cells (Figures 4L, 4M and S5J), actin nodes were robustly marked by Arl13b near the centrosome and in other cytoplasmic locations (Figures 4L, 4N and S5J). Indeed, a strong correlation (Pearson's correlation coefficients of 0.6–0.7) between Arl13b and F-actin was found in regions with actin nodes, suggesting that most Arl13b is associated with actin after CytoD treatment. Similar Arl13b-actin nodes were also visualized by β-actin, although they were less obvious due to higher overall staining as compared with F-actin (Figure S5K). Interestingly, after CytoD treatment, targeting of Arl13b to the centrosome and cilium was significantly enhanced both in growth medium and under serum-starved conditions (Figures 4H, 4I and 4O and S5K). We also used two other methods to depolymerize F-actin, in addition to CytoD. First, we used the ROCK inhibitor, Y-27632 (Liao et al., 2007), and observed similar rescue of Arl13b and INPP5E targeting in *WDR35* KO cells (Figure S6A-C). In addition, we depleted ACTR3, which is required for nucleating actin at filament branches (Kim et al., 2010; Rogers et al., 2003), and this led to increased targeting of Arl13b and INPP5E to cilia in both wild-type and *WDR35* KO cells (Figure S6D–F).

To explore the trafficking of Arl13b further, we performed live-cell imaging of Arl13b during ciliogenesis. We found that Arl13b initially accumulated at the centrosome, prior to cilium assembly and elongation (Figure 5A; Movies S1 and S2). Further, Arl13b foci were also found to transiently localize near the centrosome, indicating transport from the cytoplasm to centrosomes. Interestingly, CytoD markedly accelerated the centrosomal accumulation and cilium targeting of Arl13b (Figure 5A; Movie S2). The targeting of Arl13b to cilia was inhibited in *WDR35* KO cells (Figure 5B; Movie S3), but CytoD partially restored the rate of this transport (Figure 5B; Movie S4), consistent with our observations in fixed cells (Figure 4). By comparing transport of Arl13b in WT and *WDR35*

KO cells with and without CytoD treatment, our results show that transport of Arl13b is indeed up-regulated after actin de-polymerization.

To rule out effects of CytoD on ciliary gating of membrane proteins, we showed that the integrity of transition zone proteins, Cep290 and Tctn1 (Chih et al., 2012; Garcia-Gonzalo et al., 2011), was unaffected by Wdr35 loss or CytoD treatment (Figure S6G). In addition, a diffusion barrier exists at the base of the cilium to maintain the composition of ciliary membrane proteins, and disruption of the diffusion barrier enables free diffusion of proteins from cytoplasm to cilia (Hu et al., 2010; Kee et al., 2012). To determine whether CytoD promotes entry of membrane proteins by altering this barrier, we examined the fluorescence recovery of Alr13b inside cilia after photo-bleaching (FRAP) to test the diffusion potential of ciliary Arl13b without or with CytoD (Figures S6H and S6I). Like HTR6 and other membrane proteins (Hu et al., 2010), Arl13b in the bleached region could be partially recovered rapidly (within seconds) if either the proximal or distal region of the cilium was bleached, whereas its fluorescence was not restored within a much longer time-frame if the entire cilium was bleached (Larkins et al., 2011). A similar recovery pattern for Arl13b was observed after CytoD treatment, suggesting that Arl13b can freely diffuse inside the cilium but not across the diffusion barrier (Figures S6H and S6I). Our data suggest that the diffusion barrier is likely to be intact after CytoD treatment (Breslow et al., 2013), and CytoD promotes ciliary entry of membrane proteins like Arl13b by selective transport rather than diffusion.

Actin nodes were found to exhibit motility through a biased random walk or drift-diffusion motion (Luo et al., 2013). Given the motility of actin nodes and the observation that Arl13b is tightly associated with these nodes, we suggest that Arl13b that is not anchored to the actin bundles may be more readily transported to the centrosome/cilia, as it would possess more degrees of freedom in trafficking. Together, our data strongly suggest that defects in Wdr35-dependent membrane protein transport can be specifically rescued through actin de-polymerization (Figure S6J). In other words, the filamentous actin network suppresses transport of Wdr35-regulated membrane proteins to the centrosome and cilia in normal cells.

The impact of Wdr35 mutations on its functional interaction network

Mutations in *Wdr35* are linked to multiple recessive developmental diseases, including short-rib polydactyly as well as Sensenbrenner and Ellis-van Creveld syndromes (Bacino et al., 2012; Caparros-Martin et al., 2015; Gilissen et al., 2010; Hoffer et al., 2013; Lin et al., 2013; Mill et al., 2011). To test how such mutations could affect a Wdr35-dependent transport pathway, we expressed epitope-tagged Wdr35 disease-related and truncation mutants (all mutants analyzed, except fragments encompassing residues 641–1181 and 337–1181, are associated with disease) in an effort to rescue the defects observed in *WDR35* KO cells (Figures 6A-6D, S7A and S7B). As expected, wild-type Wdr35 efficiently targets to cilia and rescues defects in both retrograde transport of IFT88 and cilium entry of Arl13b. We found that a carboxy-terminal region of Wdr35 is required for cilium targeting, although mutations in the amino-terminus also compromised the localization of otherwise full-length proteins (Figures 6A and 6B). All mutants except E626G (which did not affect cilium assembly; (Caparros-Martin et al., 2015)) exhibited defects in transport of both IFT88 and

Arl13b (Figures 6A-D). Given that both E626G and a splice-site mutation in Wdr35 exist in the same patient (Gilissen et al., 2010), E626G could retain residual functions but may exhibit other undisclosed defects important for development. Interestingly, two carboxy-terminal Wdr35 fragments (encompassing residues 641–1181 and 337–1181) efficiently localized to cilia and showed relatively mild defects in IFT88 and Arl13b transport, as compared with an amino-terminal fragment (1–640) (Figures 6C, 6D and S7B). This suggests that the carboxy-terminal half of Wdr35 could play an important role in cargo transport. Because Wdr35 mutants with the strongest defects in retrograde IFT also exhibit the most severe defects in membrane protein entry, we surmise that retrograde transport and cargo entry into the cilium share a common mechanism.

To further elucidate how Wdr35 functions within the IFT-A complex for cargo transport, we mapped the interactions of Wdr35 disease-related and truncation mutants with membrane proteins (Arl13b and INPP5E), IFT-A subunits (IFT139, IFT122, Wdr35, and IFT43), as well as the centriolar/centriolar satellite protein, Cep290 (Figure S7*C*). Although most disease-associated point mutations generally showed mild effects, we observed several notable exceptions. First, the S168R and L531P mutations either slightly or severely altered binding to Arl13b, respectively, although binding to INPP5E was not impacted. Intriguingly, both mutations crippled binding to Cep290 altogether. Two additional mutations (W261R and Δ101–150) likewise abrogated Cep290 binding. Notably, all four mutations that disrupt Cep290 binding map to the amino-terminal WD40 repeats, which constitute known cargo-binding domains in other proteins, including subunits of Coat protein complex I (COPI), which is essential for Golgi to endoplasmic reticulum transport (Eugster et al., 2004)(see Supplemental Information). In addition, a number of Wdr35 truncation mutants (including 1–640, which also results from a patient mutation) showed dramatic alterations in binding to both IFT-A subunits and cargoes. Interestingly, the amino-terminal Wdr35 fragment (1–640) robustly interacted with Arl13b and INPP5E, but it failed to interact or exhibited considerably reduced association with IFT139, full-length Wdr35, and IFT43. On the other hand, a carboxy-terminal Wdr35 fragment (545–1181) exhibited very robust binding to cargoes and all other IFT-A subunits. Furthermore, five small, non-overlapping fragments (1–200, 201–544, 545–800, 801–954 and 955–1181) were tested, and fragment 545–800 was also found to efficiently bind to IFT122 and Arl13b. Our mapping of the Wdr35 interaction network is summarized (Figures 3H, 6E–F; Table S2), and based on the totality of these data, we suggest that Wdr35 can interact with cargoes through direct and indirect mechanisms: Wdr35 most likely interacts with membrane proteins (1) directly through its WD40 domains and (2) indirectly through associated IFT-A subunits that are likewise able to interact with these cargoes. However, the integrity of both types of Wdr35 interactions--with cargo and other IFT-A subunits--is required to fully restore the activity of this complex in *WDR35* null cells (Figure 6). In contrast with its binding to all other proteins, full-length Wdr35 was required to bind Cep290, suggesting that it interacts with the latter protein through a distinct type of interface. Interestingly, homologies between IFT-A and COPI subunits (Figures S7E and S7F) indicate similar topologies and interactions with cargoes, suggesting a resemblance in their transport mechanisms worthy of further exploration (Jekely and Arendt, 2006; Taschner et al., 2012)(See Supplemental Information).

Discussion

Model for Wdr35 function during ciliogenesis

In summary, through screening of potential Wdr35-regulated proteins in *WDR35* KO cells, we have revealed Wdr35/IFTA-dependent regulation at distinct points during ciliogenesis (Figure 6G). We propose that after Rab8 vesicle docking to the distal appendage, Wdr35 and IFT-A promote initial axoneme extension through growth of Rab8 vesicles. IFT-B, BBsome, and transition zone protein are correctly targeted independently of IFT-A. Further, the IFT-A complex also transports various membrane proteins to cilia, whereas the actin network dampens IFT-A-dependent vesicular and membrane protein transport. After cilium entry, IFT-A, IFT-B, BBSome, and membrane protein cargoes are regulated by IFT-A-mediated retrograde IFT from the cilium tip to the base. Interestingly, all modes of Wdr35-dependent transport that we have characterized in this study are directed toward the centrosomal base, suggesting a unified mechanism for microtubule minus-end directed transport, possibly involving distinct dynein complexes. Retrograde IFT and transport to the centriolar satellites are indeed known to be directed by different dynein motors (Cole and Snell, 2009; Hao et al., 2011).

Role for the actin cytoskeleton in ciliogenesis

Actin de-polymerization has been shown to stabilize the pericentrosomal preciliary compartment (PPC) (Kim et al., 2015; Kim et al., 2010), a vesiculo-tubular compartment that collects proteins destined for the cilium at the early stages of ciliogenesis. Our data indicate that CytoD promotes cilium entry of several membrane and vesicle proteins, although it is currently unclear whether and how these proteins partition with PPC components. A recent study suggested that Arl13b interacts with an exocyst component, Sec5, which localizes to both cilia and the periciliary region in MDCK cells (Seixas et al., 2015). Nonetheless, Sec5 was not found in all Arl13b-positive cilia of RPE1 and NIH-3T3 cells (Seixas et al., 2015), suggesting that membrane transport could differ across cell types. Arl13b was found to co-localize and interact with actin in our study and in HeLa cells (Barral et al., 2012), and here we also show that actin de-polymerization leads to both conversion of Arl13b-actin bundles to dissociated Arl13b-actin nodes and enhanced targeting of Arl13b to centrosome and cilia. Therefore, we hypothesize that assembly of actin filaments can antagonize Wdr35-dependent transport during cilium assembly, and CytoD releases Arl13b from the filamentous actin network into Arl13b-actin nodes for transport toward the centrosome/cilium by diffusion-drift motion, bypassing the function of Wdr35. We note that only specific types of actin-associated proteins (e.g., myosin II) show clear association with actin nodes after actin depolymerization, like Arl13b, although others (α-actinin and β-spectrin) do not (Luo et al., 2013). Further studies will be required to understand how Wdr35 and Arl13b collaborate with other actin-binding proteins, if any, to control ciliogenesis-dependent transport in the face of an intact filamentous actin network.

Moreover, the potential utility of actin-depolymerizing drugs in the treatment of ciliopathies caused by mutations in genes encoding IFT-A proteins, such as *WDR35*, should also be explored. Loss of *WDR35* leads to defects in trafficking of several GPCR pathway components, including the serotonin receptor and the Hedgehog component, Smo.

Hedgehog signaling is essential for chondrocyte differentiation and osteogenesis during bone growth, mesenchymal cell differentiation during skeletal repair and regeneration, and normal limb bud patterning, and serotonin was found to trigger changes in cell adhesiveness and ectoderm extension (Alman, 2015; Bouldin et al., 2010; Colas et al., 1999). Our functional studies of Wdr35 could therefore help link the ectodermal and skeletal abnormalities found in Sensenbrenner patients, as well as other clinical manifestations associated with defects in other IFT-A components, with Wdr35 mutations (Gilissen et al., 2010).

Experimental Procedures

Generation of *WDR35* Knock-out RPE1 and 293T cells by CRISPR/Cas9

Generation of CRISPR knockout (KO) cells was previously described (Ran et al., 2013; Sanjana et al., 2014). In brief, lentiGuide-Puro empty vector was used to generate CRISPR control cells, and lentiGuide-Puro ligated with two different guide RNAs (gRNA-1 and gRNA-2) targeting 5'-GAGCAAGAAAGTGAGTTTCC-3' in exon 1 and 5'-CCGCATGCTATGAACCCTTG-3' in exon 2 were used to generate *WDR35* knockout #1 and #2, respectively. Lentivirus supernatants from 293T cells transfected with lentiCas9-Blast and lentiGuide-Puro vectors were added to RPE1 cells for virus infection. After one week of infection, knockout effectiveness was verified by Surveyor assay, and single clones were isolated. The genomic regions around the CRISPR targeting sites were amplified and sequenced, and one control clone and two *WDR35* KO clones with predicted premature translation termination were selected for further functional analysis. The Cas9-Flag could not be detected by immunofluorescence in both control and the two *WDR35* KO clones in this study. Similarly, *WDR35* KO 293T cells were generated with gRNA-2 and a modified pLVX-Cas9 expression vector. Targeted genomic regions in wild type and knockout clones were further verified by sequencing.

Detailed descriptions of the other experimental procedures used in this study are available in the Supplemental Information.

Supplementary Material

Refer to Web version on PubMed Central for supplementary material.

Acknowledgments

We are very grateful to the following researchers who have shared plasmids and antibodies: Heleen H. Arts (Radboud University Nijmegen Medical Centre, Netherlands), Steve Caplan (University of Nebraska Medical Center, USA), Shuhei Chiba (Tohoku University, Japan), Erica E. Davis (Duke University Medical Center, USA), Jonathan Eggenschwile (University of Georgia, USA), Joseph G. Gleeson (Rockefeller University, USA), Peter K. Jackson (Stanford University School of Medicine, USA), Toshiaki Katada (University of Tokyo, Japan), Nicholas Katsanis (Duke University Medical Center, USA), Kensaku Mizuno (Tohoku University, Japan), Kunsoo Rhee (Seoul National University, Korea), Johan Peränen (University of Helsinki, Finland), Rytis Prekeris (University of Colorado, USA), Jeremy F. Reiter (University of California, San Francisco, USA), Ronald Roepman (Radboud University Nijmegen Medical Centre, Netherlands), Seongjin Seo (University of Iowa, USA), Tang K. Tang (Institute of Biomedical Sciences, Taiwan), and Mark von Zastrow (University of California, San Francisco, USA). We thank Kristen Dancel, Chris Petzold, and Feng-Xia Liang at the NYU Imaging Center for help with electron microscopy. Work in BDD's laboratory was supported by NIH grants HD069647 and R01 GM 120776-05A1. B.D.D. dedicates this work to the memory of Zdzislaw (Sigmund) Dynlacht.

References

Ahmed NT, Gao C, Lucker BF, Cole DG, Mitchell DR. ODA16 aids axonemal outer row dynein assembly through an interaction with the intraflagellar transport machinery. The Journal of cell biology. 2008; 183:313–322. [PubMed: 18852297]

Alazami AM, Seidahmed MZ, Alzahrani F, Mohammed AO, Alkuraya FS. Novel IFT122 mutation associated with impaired ciliogenesis and cranioectodermal dysplasia. Molecular genetics & genomic medicine. 2014; 2:103–106. [PubMed: 24689072]

Alman BA. The role of hedgehog signalling in skeletal health and disease. Nature reviews Rheumatology. 2015; 11:552–560. [PubMed: 26077918]

Bacino CA, Dhar SU, Brunetti-Pierri N, Lee B, Bonnen PE. WDR35 mutation in siblings with Sensenbrenner syndrome: a ciliopathy with variable phenotype. American journal of medical genetics Part A. 2012; 158A:2917–2924. [PubMed: 22987818]

Barral DC, Garg S, Casalou C, Watts GF, Sandoval JL, Ramalho JS, Hsu VW, Brenner MB. Arl13b regulates endocytic recycling traffic. Proceedings of the National Academy of Sciences of the United States of America. 2012; 109:21354–21359. [PubMed: 23223633]

Bhogaraju S, Cajanek L, Fort C, Blisnick T, Weber K, Taschner M, Mizuno N, Lamla S, Bastin P, Nigg EA, et al. Molecular basis of tubulin transport within the cilium by IFT74 and IFT81. Science. 2013a; 341:1009–1012. [PubMed: 23990561]

Bhogaraju S, Engel BD, Lorentzen E. Intraflagellar transport complex structure and cargo interactions. Cilia. 2013b; 2:10. [PubMed: 23945166]

Blacque OE, Li C, Inglis PN, Esmail MA, Ou G, Mah AK, Baillie DL, Scholey JM, Leroux MR. The WD repeat-containing protein IFTA-1 is required for retrograde intraflagellar transport. Molecular biology of the cell. 2006; 17:5053–5062. [PubMed: 17021254]

Bouldin CM, Gritli-Linde A, Ahn S, Harfe BD. Shh pathway activation is present and required within the vertebrate limb bud apical ectodermal ridge for normal autopod patterning. Proceedings of the National Academy of Sciences of the United States of America. 2010; 107:5489–5494. [PubMed: 20212115]

Breslow DK, Koslover EF, Seydel F, Spakowitz AJ, Nachury MV. An in vitro assay for entry into cilia reveals unique properties of the soluble diffusion barrier. The Journal of cell biology. 2013; 203:129–147. [PubMed: 24100294]

Cao J, Shen Y, Zhu L, Xu Y, Zhou Y, Wu Z, Li Y, Yan X, Zhu X. miR-129–3p controls cilia assembly by regulating CP110 and actin dynamics. Nature cell biology. 2012; 14:697–706. [PubMed: 22684256]

Caparros-Martin JA, De Luca A, Cartault F, Aglan M, Temtamy S, Otaify GA, Mehrez M, Valencia M, Vazquez L, Alessandri JL, et al. Specific variants in WDR35 cause a distinctive form of Ellis-van Creveld syndrome by disrupting the recruitment of the EvC complex and SMO into the cilium. Human molecular genetics. 2015; 24:4126–4137. [PubMed: 25908617]

Cevik S, Sanders AA, Van Wijk E, Boldt K, Clarke L, van Reeuwijk J, Hori Y, Horn N, Hetterschijt L, Wdowicz A, et al. Active transport and diffusion barriers restrict Joubert Syndrome-associated ARL13B/ARL-13 to an Inv-like ciliary membrane subdomain. PLoS genetics. 2013; 9:e1003977. [PubMed: 24339792]

Chih B, Liu P, Chinn Y, Chalouni C, Komuves LG, Hass PE, Sandoval W, Peterson AS. A ciliopathy complex at the transition zone protects the cilia as a privileged membrane domain. Nature cell biology. 2012; 14:61–72.

Colas JF, Launay JM, Vonesch JL, Hickel P, Maroteaux L. Serotonin synchronises convergent extension of ectoderm with morphogenetic gastrulation movements in Drosophila. Mechanisms of development. 1999; 87:77–91. [PubMed: 10495273]

Cole DG, Snell WJ. SnapShot: Intraflagellar transport. Cell. 2009; 137:784–784. e781. [PubMed: 19450523]

Cong L, Ran FA, Cox D, Lin S, Barretto R, Habib N, Hsu PD, Wu X, Jiang W, Marraffini LA, et al. Multiplex genome engineering using CRISPR/Cas systems. Science. 2013; 339:819–823. [PubMed: 23287718]

Corbit KC, Aanstad P, Singla V, Norman AR, Stainier DY, Reiter JF. Vertebrate Smoothened functions at the primary cilium. Nature. 2005; 437:1018–1021. [PubMed: 16136078]

Eguether T, San Agustin JT, Keady BT, Jonassen JA, Liang Y, Francis R, Tobita K, Johnson CA, Abdelhamed ZA, Lo CW, et al. IFT27 links the BBSome to IFT for maintenance of the ciliary signaling compartment. Developmental cell. 2014; 31:279–290. [PubMed: 25446516]

Engel BD, Ishikawa H, Wemmer KA, Geimer S, Wakabayashi K, Hirono M, Craige B, Pazour GJ, Witman GB, Kamiya R, et al. The role of retrograde intraflagellar transport in flagellar assembly, maintenance, and function. The Journal of cell biology. 2012; 199:151–167. [PubMed: 23027906]

Eugster A, Frigerio G, Dale M, Duden R. The alpha- and beta'-COP WD40 domains mediate cargo-selective interactions with distinct di-lysine motifs. Molecular biology of the cell. 2004; 15:1011–1023. [PubMed: 14699056]

Fu W, Asp P, Canter B, Dynlacht BD. Primary cilia control hedgehog signaling during muscle differentiation and are deregulated in rhabdomyosarcoma. Proceedings of the National Academy of Sciences of the United States of America. 2014; 111:9151–9156. [PubMed: 24927541]

Garcia-Gonzalo FR, Corbit KC, Sirerol-Piquer MS, Ramaswami G, Otto EA, Noriega TR, Seol AD, Robinson JF, Bennett CL, Josifova DJ, et al. A transition zone complex regulates mammalian ciliogenesis and ciliary membrane composition. Nature genetics. 2011; 43:776–784. [PubMed: 21725307]

Gilissen C, Arts HH, Hoischen A, Spruijt L, Mans DA, Arts P, van Lier B, Steehouwer M, van Reeuwijk J, Kant SG, et al. Exome sequencing identifies WDR35 variants involved in Sensenbrenner syndrome. American journal of human genetics. 2010; 87:418–423. [PubMed: 20817137]

Hao L, Thein M, Brust-Mascher I, Civelekoglu-Scholey G, Lu Y, Acar S, Prevo B, Shaham S, Scholey JM. Intraflagellar transport delivers tubulin isotypes to sensory cilium middle and distal segments. Nature cell biology. 2011; 13:790–798. [PubMed: 21642982]

Hao LM, Scholey JM. Intraflagellar transport at a glance. Journal of cell science. 2009; 122:889–892. [PubMed: 19295122]

Haurwitz RE, Jinek M, Wiedenheft B, Zhou K, Doudna JA. Sequence- and structure-specific RNA processing by a CRISPR endonuclease. Science. 2010; 329:1355–1358. [PubMed: 20829488]

Hoffer JL, Fryssira H, Konstantinidou AE, Ropers HH, Tzschach A. Novel WDR35 mutations in patients with cranioectodermal dysplasia (Sensenbrenner syndrome). Clinical genetics. 2013; 83:92–95. [PubMed: 22486404]

Hou Y, Qin H, Follit JA, Pazour GJ, Rosenbaum JL, Witman GB. Functional analysis of an individual IFT protein: IFT46 is required for transport of outer dynein arms into flagella. The Journal of cell biology. 2007; 176:653–665. [PubMed: 17312020]

Hu Q, Milenkovic L, Jin H, Scott MP, Nachury MV, Spiliotis ET, Nelson WJ. A septin diffusion barrier at the base of the primary cilium maintains ciliary membrane protein distribution. Science. 2010; 329:436–439. [PubMed: 20558667]

Humbert MC, Weihbrecht K, Searby CC, Li Y, Pope RM, Sheffield VC, Seo S. ARL13B, PDE6D, and CEP164 form a functional network for INPP5E ciliary targeting. Proceedings of the National Academy of Sciences of the United States of America. 2012; 109:19691–19696. [PubMed: 23150559]

Jekely G, Arendt D. Evolution of intraflagellar transport from coated vesicles and autogenous origin of the eukaryotic cilium. BioEssays : news and reviews in molecular, cellular and developmental biology. 2006; 28:191–198.

Kee HL, Dishinger JF, Blasius TL, Liu CJ, Margolis B, Verhey KJ. A size-exclusion permeability barrier and nucleoporins characterize a ciliary pore complex that regulates transport into cilia. Nature cell biology. 2012; 14:431–437. [PubMed: 22388888]

Kim J, Jo H, Hong H, Kim MH, Kim JM, Lee JK, Heo WD, Kim J. Actin remodelling factors control ciliogenesis by regulating YAP/TAZ activity and vesicle trafficking. Nature communications. 2015; 6:6781.

Kim J, Krishnaswami SR, Gleeson JG. CEP290 interacts with the centriolar satellite component PCM-1 and is required for Rab8 localization to the primary cilium. Human molecular genetics. 2008; 17:3796–3805. [PubMed: 18772192]

Kim J, Lee JE, Heynen-Genel S, Suyama E, Ono K, Lee K, Ideker T, Aza-Blanc P, Gleeson JG. Functional genomic screen for modulators of ciliogenesis and cilium length. Nature. 2010; 464:1048–1051. [PubMed: 20393563]

Kim JC, Badano JL, Sibold S, Esmail MA, Hill J, Hoskins BE, Leitch CC, Venner K, Ansley SJ, Ross AJ, et al. The Bardet-Biedl protein BBS4 targets cargo to the pericentriolar region and is required for microtubule anchoring and cell cycle progression. Nature genetics. 2004; 36:462–470. [PubMed: 15107855]

Kobayashi T, Kim S, Lin YC, Inoue T, Dynlacht BD. The CP110-interacting proteins Talpid3 and Cep290 play overlapping and distinct roles in cilia assembly. The Journal of cell biology. 2014; 204:215–229. [PubMed: 24421332]

Kovacs JJ, Whalen EJ, Liu R, Xiao K, Kim J, Chen M, Wang J, Chen W, Lefkowitz RJ. Beta-arrestin-mediated localization of smoothened to the primary cilium. Science. 2008; 320:1777–1781. [PubMed: 18497258]

Larkins CE, Aviles GD, East MP, Kahn RA, Caspary T. Arl13b regulates ciliogenesis and the dynamic localization of Shh signaling proteins. Molecular biology of the cell. 2011; 22:4694–4703. [PubMed: 21976698]

Lechtreck KF. IFT-Cargo Interactions and Protein Transport in Cilia. Trends in biochemical sciences. 2015; 40:765–778. [PubMed: 26498262]

Li Y, Wei Q, Zhang Y, Ling K, Hu J. The small GTPases ARL-13 and ARL-3 coordinate intraflagellar transport and ciliogenesis. The Journal of cell biology. 2010; 189:1039–1051. [PubMed: 20530210]

Liao JK, Seto M, Noma K. Rho kinase (ROCK) inhibitors. Journal of cardiovascular pharmacology. 2007; 50:17–24. [PubMed: 17666911]

Liem KF Jr, Ashe A, He M, Satir P, Moran J, Beier D, Wicking C, Anderson KV. The IFT-A complex regulates Shh signaling through cilia structure and membrane protein trafficking. The Journal of cell biology. 2012; 197:789–800. [PubMed: 22689656]

Liew GM, Ye F, Nager AR, Murphy JP, Lee JS, Aguiar M, Breslow DK, Gygi SP, Nachury MV. The intraflagellar transport protein IFT27 promotes BBSome exit from cilia through the GTPase ARL6/BBS3. Developmental cell. 2014; 31:265–278. [PubMed: 25443296]

Lin AE, Traum AZ, Sahai I, Keppler-Noreuil K, Kukolich MK, Adam MP, Westra SJ, Arts HH. Sensenbrenner syndrome (Cranioectodermal dysplasia): clinical and molecular analyses of 39 patients including two new patients. American journal of medical genetics Part A. 2013; 161A: 2762–2776. [PubMed: 24123776]

Lu Q, Insinna C, Ott C, Stauffer J, Pintado PA, Rahajeng J, Baxa U, Walia V, Cuenca A, Hwang YS, et al. Early steps in primary cilium assembly require EHD1/EHD3-dependent ciliary vesicle formation. Nature cell biology. 2015; 17:228–240. [PubMed: 25686250]

Luo W, Yu CH, Lieu ZZ, Allard J, Mogilner A, Sheetz MP, Bershadsky AD. Analysis of the local organization and dynamics of cellular actin networks. The Journal of cell biology. 2013; 202:1057–1073. [PubMed: 24081490]

Lykke-Andersen S, Jensen TH. Nonsense-mediated mRNA decay: an intricate machinery that shapes transcriptomes. Nature reviews Molecular cell biology. 2015; 16:665–677. [PubMed: 26397022]

Mill P, Lockhart PJ, Fitzpatrick E, Mountford HS, Hall EA, Reijns MA, Keighren M, Bahlo M, Bromhead CJ, Budd P, et al. Human and mouse mutations in WDR35 cause short-rib polydactyly syndromes due to abnormal ciliogenesis. American journal of human genetics. 2011; 88:508–515. [PubMed: 21473986]

Mukhopadhyay S, Wen X, Chih B, Nelson CD, Lane WS, Scales SJ, Jackson PK. TULP3 bridges the IFT-A complex and membrane phosphoinositides to promote trafficking of G protein-coupled receptors into primary cilia. Genes & development. 2010; 24:2180–2193. [PubMed: 20889716]

Nozawa YI, Lin C, Chuang PT. Hedgehog signaling from the primary cilium to the nucleus: an emerging picture of ciliary localization, trafficking and transduction. Current opinion in genetics & development. 2013; 23:429–437. [PubMed: 23725801]

Ocbina PJ, Eggenschwiler JT, Moskowitz I, Anderson KV. Complex interactions between genes controlling trafficking in primary cilia. Nature genetics. 2011; 43:547–553. [PubMed: 21552265]

Perrault I, Saunier S, Hanein S, Filhol E, Bizet AA, Collins F, Salih MA, Gerber S, Delphin N, Bigot K, et al. Mainzer-Saldino syndrome is a ciliopathy caused by IFT140 mutations. American journal of human genetics. 2012; 90:864–870. [PubMed: 22503633]

Qin JA, Lin YL, Norman RX, Ko HW, Eggenschwiler JT. Intraflagellar transport protein 122 antagonizes Sonic Hedgehog signaling and controls ciliary localization of pathway components. Proceedings of the National Academy of Sciences of the United States of America. 2011; 108:1456–1461. [PubMed: 21209331]

Ran FA, Hsu PD, Wright J, Agarwala V, Scott DA, Zhang F. Genome engineering using the CRISPR-Cas9 system. Nature protocols. 2013; 8:2281–2308. [PubMed: 24157548]

Rogers SL, Wiedemann U, Stuurman N, Vale RD. Molecular requirements for actin-based lamella formation in Drosophila S2 cells. The Journal of cell biology. 2003; 162:1079–1088. [PubMed: 12975351]

Sanjana NE, Shalem O, Zhang F. Improved vectors and genome-wide libraries for CRISPR screening. Nature methods. 2014; 11:783–784. [PubMed: 25075903]

Seixas C, Choi SY, Polgar N, Umberger NL, East MP, Zuo X, Moreiras H, Ghossoub R, Benmerah A, Kahn RA, et al. Arl13b and the exocyst interact synergistically in ciliogenesis. Molecular biology of the cell. 2015

Taschner M, Bhogaraju S, Lorentzen E. Architecture and function of IFT complex proteins in ciliogenesis. Differentiation; research in biological diversity. 2012; 83:S12–22. [PubMed: 22118932]

Thomas S, Wright KJ, Le Corre S, Micalizzi A, Romani M, Abhyankar A, Saada J, Perrault I, Amiel J, Litzler J, et al. A homozygous PDE6D mutation in Joubert syndrome impairs targeting of farnesylated INPP5E protein to the primary cilium. Human mutation. 2014; 35:137–146. [PubMed: 24166846]

Tran PV, Haycraft CJ, Besschetnova TY, Turbe-Doan A, Stottmann RW, Herron BJ, Chesebro AL, Qiu H, Scherz PJ, Shah JV, et al. THM1 negatively modulates mouse sonic hedgehog signal transduction and affects retrograde intraflagellar transport in cilia. Nature genetics. 2008; 40:403–410. [PubMed: 18327258]

Tsang WY, Bossard C, Khanna H, Peranen J, Swaroop A, Malhotra V, Dynlacht BD. CP110 suppresses primary cilia formation through its interaction with CEP290, a protein deficient in human ciliary disease. Developmental cell. 2008; 15:187–197. [PubMed: 18694559]

Westlake CJ, Baye LM, Nachury MV, Wright KJ, Ervin KE, Phu L, Chalouni C, Beck JS, Kirkpatrick DS, Slusarski DC, et al. Primary cilia membrane assembly is initiated by Rab11 and transport protein particle II (TRAPPII) complex-dependent trafficking of Rabin8 to the centrosome. Proceedings of the National Academy of Sciences of the United States of America. 2011; 108:2759–2764. [PubMed: 21273506]

Highlights

- Wdr35 regulates selective transport of distinct cargoes for primary cilium assembly
- Wdr35 regulates cargo transport in concert with other IFT-A subunits
- Actin depolymerization increases Wdr35-dependent membrane cargo transport
- Defects in IFT-A mediated cargo transport are linked with disease

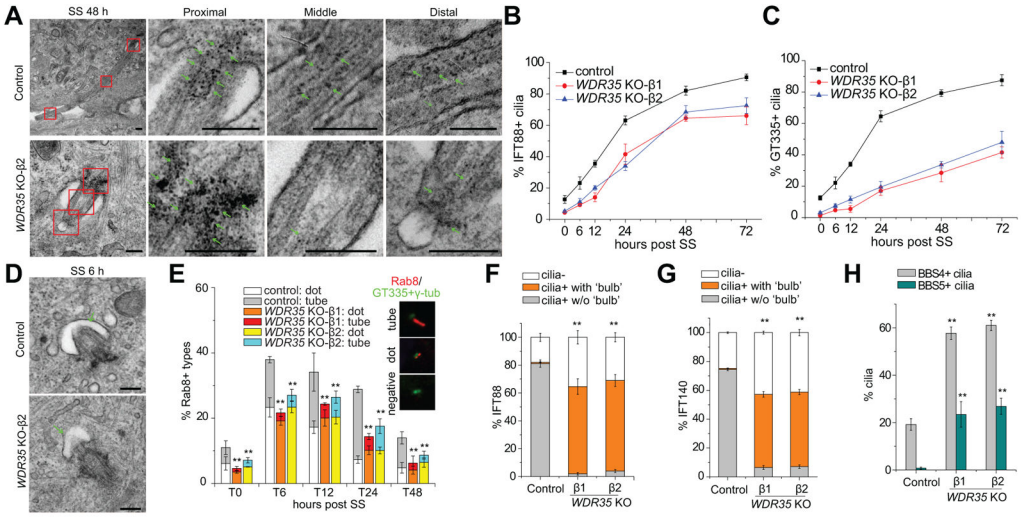

Figure 1. Wdr35 is essential for proper cilium assembly, retrograde transport, and cargo export

(A) Primary cilium structure in control and *WDR35* KO #2 cells was examined by transmission electron microscopy (TEM) after 48 h of serum-starvation (SS). Magnified views of the boxed insets indicate the proximal, middle and distal regions of the cilia. Green arrows indicate electron-dense particles inside cilia. (B and C) Percentages of IFT88- (B) and GT335-positive (C) cilia in *WDR35* KO versus control cells at different time points are shown. (D) Ciliary vesicles in *WDR35* KO cells at 6 h after SS are indicated with arrows. (E) Rab8-positive (Rab+) vesicles near centrosomes/cilia were classified and counted at different time points before and after SS. Asterisks indicate significance of occurrence of Rab8 tubes. (F and G) Percentages of different IFT88 (F) and IFT140 (G) patterns at cilia in control and *WDR35* KO cells. The aberrant accumulation of protein (e.g., IFT88) inside cilia, mostly at the tip, is noted as 'bulb', and significance is indicated with asterisk. (H) Quantification of BBS4- and BBS5-positive cilia in control and *WDR35* KO cells. Scale bars in (A) and (D), 0.2 μm. All data are presented as mean ± SD. $^{**}P < 0.01$. **See also** Figures S1 and S2, and Table S1.

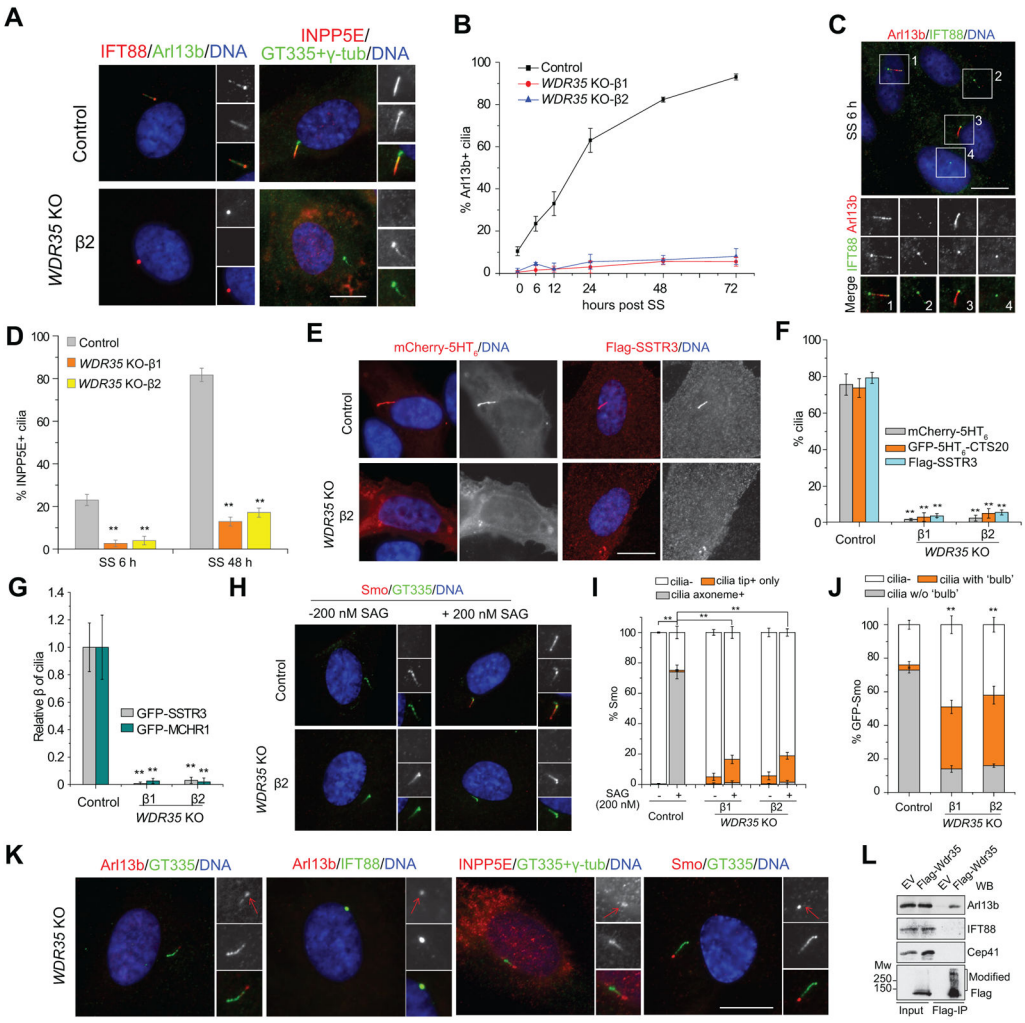

Figure 2. Wdr35 controls membrane protein transport into cilia

(A) Ciliary membrane proteins (Arl13b and INPP5E) were visualized in serum-starved control and *WDR35* KO RPE1 cells. (B) Arl13b+ cilia were quantified at different times after serum starvation. (C) RPE1 cells at SS 6 h were co-stained with Arl13b and IFT88 antibodies. Boxed insets with different patterns of IFT88 and Arl13b staining are shown. Boxes 1 to 4 indicate tubular structures that are Arl13b+IFT88+, Arl13b-IFT88+, Arl13b +IFT88−, and Arl13b−IFT88−, respectively. (D) INPP5E+ cilia were quantified at different times. (E) Representative images showing control and *WDR35* KO cells transfected with mCherry-5HT$_6$ or Flag-SSTR3. (F) Quantification of mCherry-5HT$_6$+, GFP-5HT$_6$−CTS20+ and Flag-SSTR3+ cilia after Wdr35 ablation. (G) Control and *WDR35* KO cells were infected with retroviruses expressing GFP-SSTR3 or GFP-MCHR1, and relative numbers of GFP+ cilia were quantified. (H) Control and *WDR35* KO cells with or without sonic hedgehog agonist (SAG) treatment were visualized with anti-Smo antibodies. (I) Quantification of Smo staining in (H). Asterisks indicate significance of occurrence of Smo+ cilia. (J) GFP-Smo was visualized after transfecting WDR35 KO cells, and the staining pattern of GFP-Smo was quantified. Asterisks indicate significance of occurrence of cilia with bulbous Smo. (K) Representative images of *WDR35* KO cells showing that Arl13b,

INPP5E and Smo are also regulated by Wdr35-dependent retrograde transport. The red arrows indicate the aberrant protein accumulation at cilia tips. (L) Lysates of proliferating 293T cells transfected with empty vector or Flag-Wdr35 were immunoprecipitated (IP) using anti-Flag antibodies. Western blots of immunoprecipitates were probed with antibodies against Arl13b, IFT88, Cep41, and Flag, as shown. The reduced mobility of modified (likely ubiquitylated; data not shown) Wdr35 is shown. Scale bar, 10 μm. Data are presented as mean ± SD. $^{**}P < 0.01$. In all cases, the cells were fixed at 48 h after SS to stain cilia unless stated otherwise. **See also** Figure S2 and Table S1.

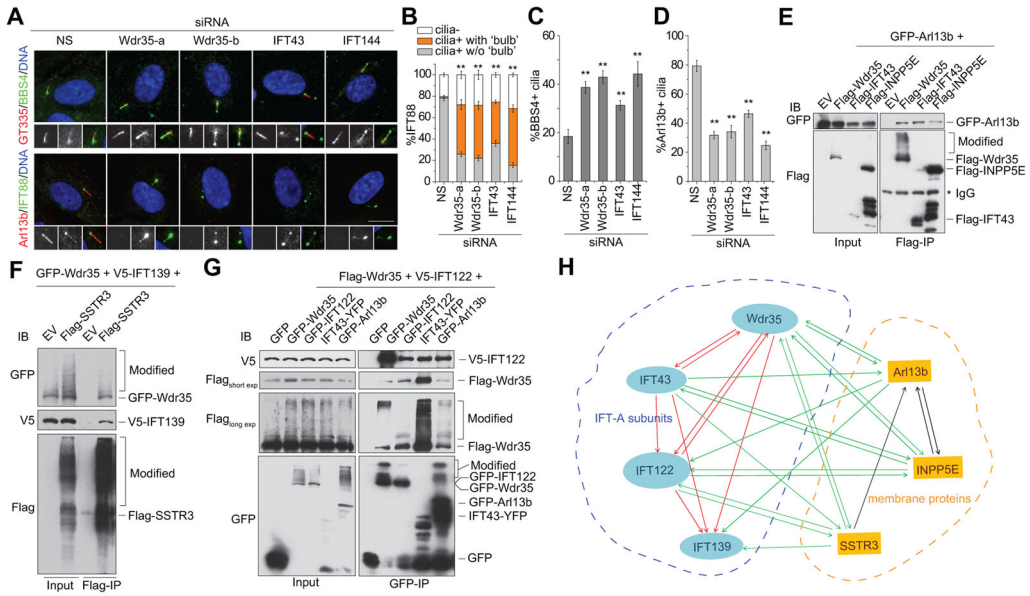

Figure 3. Wdr35 regulates cargo transport in concert with other IFT-A subunits

(A) RPE1 cells transfected with non-specific (NS) siRNAs and siRNAs targeting different IFT-A subunits (Wdr35, IFT43, and IFT144) were serum starved for 48 h and stained with GT335, BBS4, Arl13b and IFT88 antibodies as indicated. Two different Wdr35 oligos (a and b) were used. Representative immunofluorescence images are shown. Scale bar, 10 μm. (B) Quantification of IFT88 phenotypes at cilia as in (A). Asterisks indicate significance of occurrence of bulbous IFT88. (C and D) Quantification of BBS4+ (C) and Arl13b+ (D) cilia as in (A). Data in (B–D) are presented as mean ± SD. $^{**}P < 0.01$. (E) Lysates of 293T cells co-transfected with GFP-Arl13b and either Flag-EV, Flag-Wdr35, Flag-IFT43, or Flag-INPP5E were immunoprecipitated (IP) using anti-Flag antibodies. Both inputs and IPs were probed with antibodies against GFP and Flag antibodies. (F) As in (E), extracts of cells co-transfected with GFP-Wdr35, V5-IFT139, and either Flag-EV or Flag SSTR3, were immunoprecipitated using anti-Flag antibodies. Blots were probed with anti-GFP, anti-V5, and anti-Flag antibodies as shown. (G) 293T cells expressing Flag-Wdr35, V5–122, and each of five GFP/YFP-tagged vectors (GFP alone, GFP-Wdr35, GFP-IFT122, IFT43-YFP and GFP-Arl13b) were lysed and immunoprecipitated using anti-GFP as in (E and F). Blots were probed with antibodies against V5, Flag, and GFP. The bands on the blots are annotated on the right in (E–G), and the smears indicate modified forms of proteins. (H) Summary of interactions among four IFT-A subunits (Wdr35, IFT43, IFT122 and IFT139) and three ciliary membrane cargo proteins (Arl13b, INPP5E and SSTR3), indicated by blue and yellow dotted lines, respectively. Interactions between two IFT-A subunits, two membrane proteins, and one IFT-A subunit and one membrane protein are indicated with red, blue, and green arrows, respectively. **See also** Figures S3 and S4.

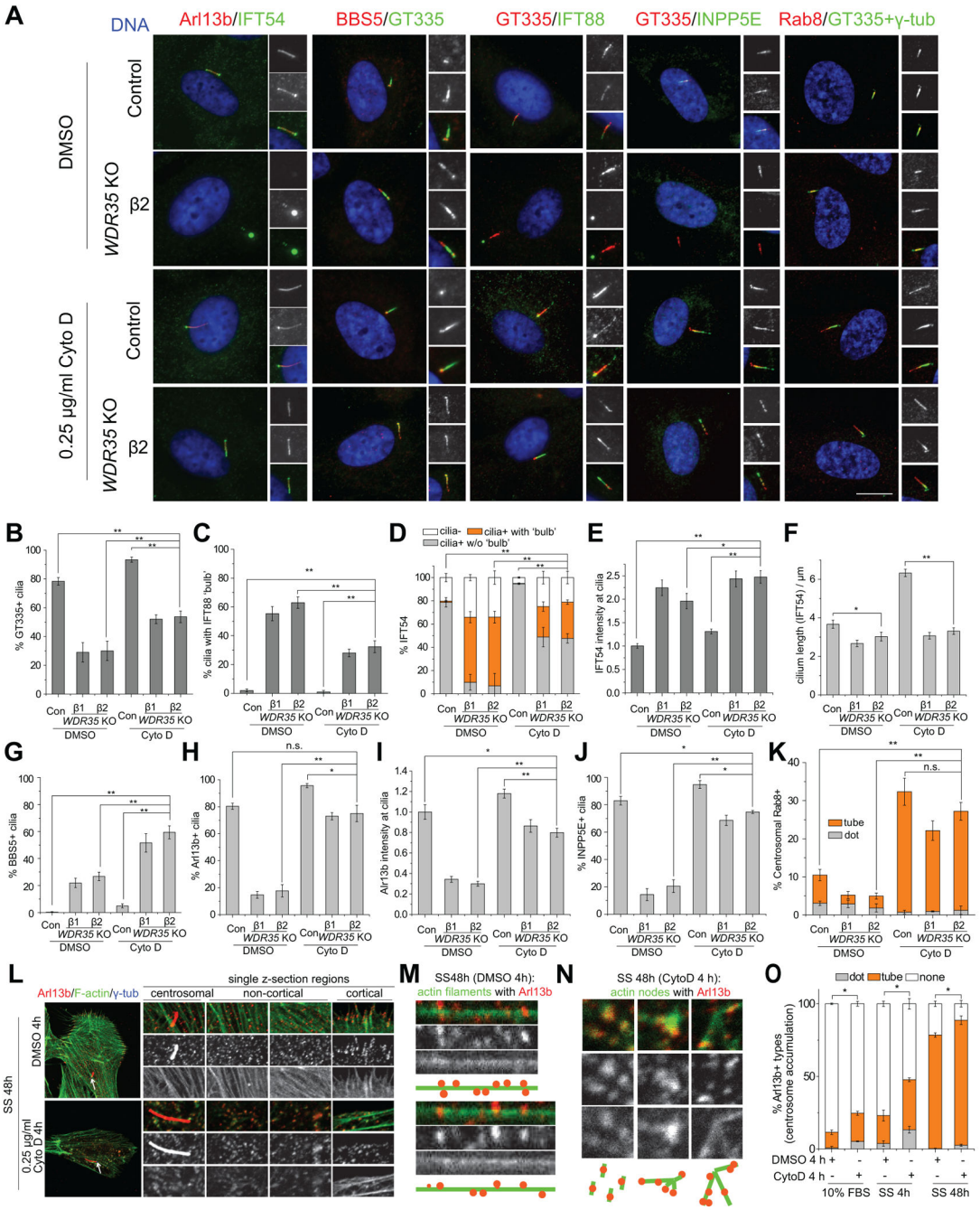

Figure 4. The actin network antagonizes cargo transport

(A) Control and *WDR35* KO cells treated with DMSO or 0.25 μg/ml Cytochalasin D for 24 h were visualized with antibodies against cilium markers, GT335, IFT54, IFT88, BBS5, and Arl13b. Representative immunofluorescence images are shown. Scale bar, 10 μm. (B–K) Quantification of cilium markers as in (A). GT335+ cilia (B), cilia with IFT88+ 'bulb' (C), IFT54 localization at cilia (D), relative IFT54 immunofluorescence intensity at cilia (E), cilium length measured by IFT54 (F), percentages of BBS5+ cilia (G), percentages of Arl13b+ cilia (H), Arl13b intensity at cilia (I), percentages of INPP5E+ cilia (J), and

percentages of centrosomal Rab8 types (K) were analyzed. Asterisks in (D) indicate significance of occurrence of the bulbous IFT54. (L) RPE1 cells starved for 48 h (and treated with DMSO or CytoD for the final 4 h) were stained with anti-Arl13b antibodies and phalloidin-FITC. Representative single z-sections of different cellular regions are shown. Arrows indicate centrosomes visualized by γ-tubulin. (M and N) Visualized Arl13b-actin complex types in non-cortical regions as in (L). Both representative images and their illustrated cartoons are shown. Arl13b associated with long actin filaments when treated with DMSO (M) while co-localize with small actin nodes with CytoD treatment (N). (O) Arl13b-positive (Arl13b+) structures (dot/tube) around centrosomes were counted in RPE1 cells with DMSO or CytoD treatment as indicated. Asterisks indicate significance of occurrence of total Arl13b+ structures. Data in (E), (F) and (I) are presented as mean ± SEM, and others are shown as mean ± SD. $^{**}P < 0.01$; $^{*}P < 0.05$; n.s., not significant. **See also** Figures S5 and S6.

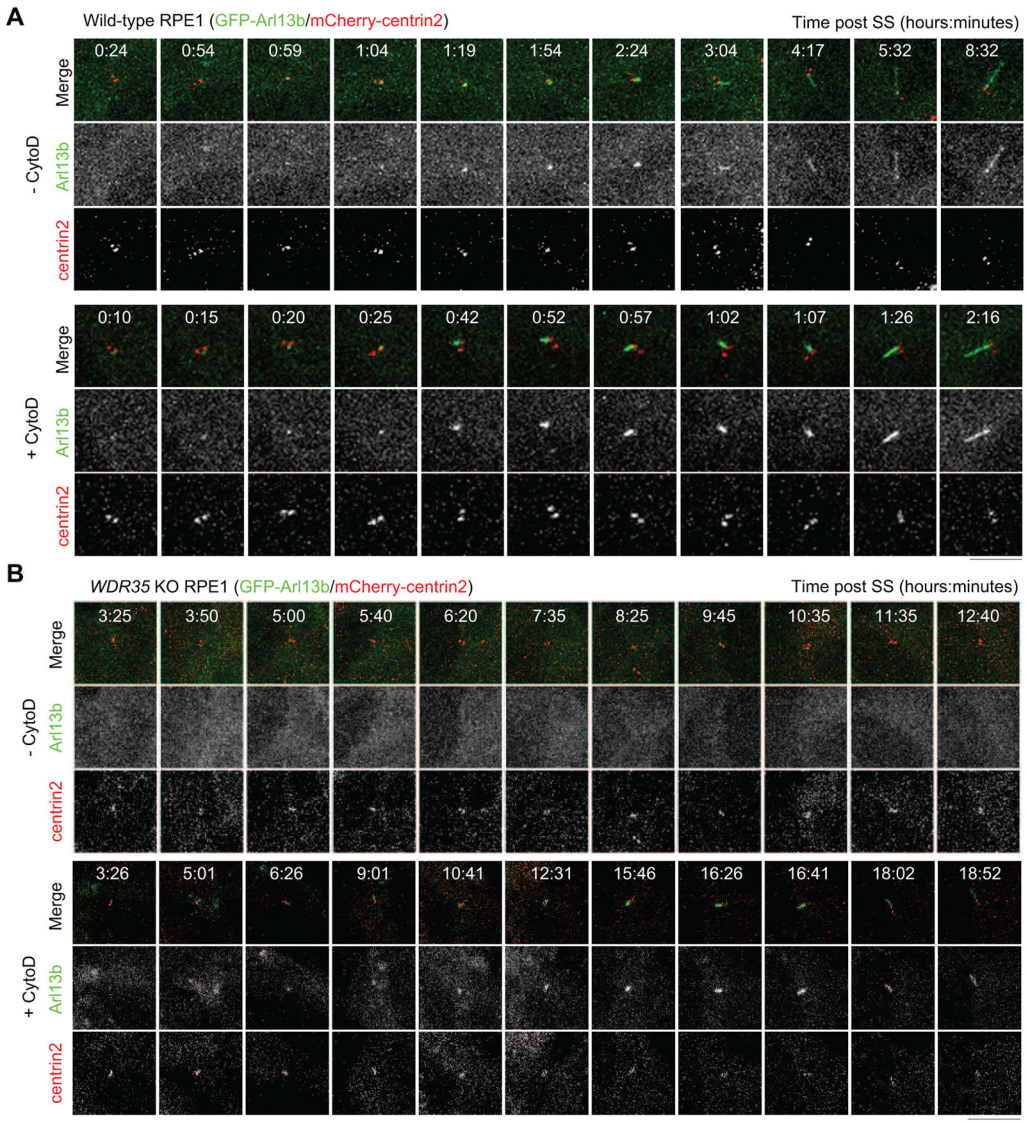

Figure 5. Cytochalasin D promotes active transport of Arl13b to the centrosome and cilium

(A and B) Wild type (A) and *WDR35* KO (B) RPE1 cells expressing GFP-Arl13b and mCherry-centrin2 were serum-starved in medium without or with CytoD. Representative images at indicated time points were shown. **See also** Figures S5 and S6.

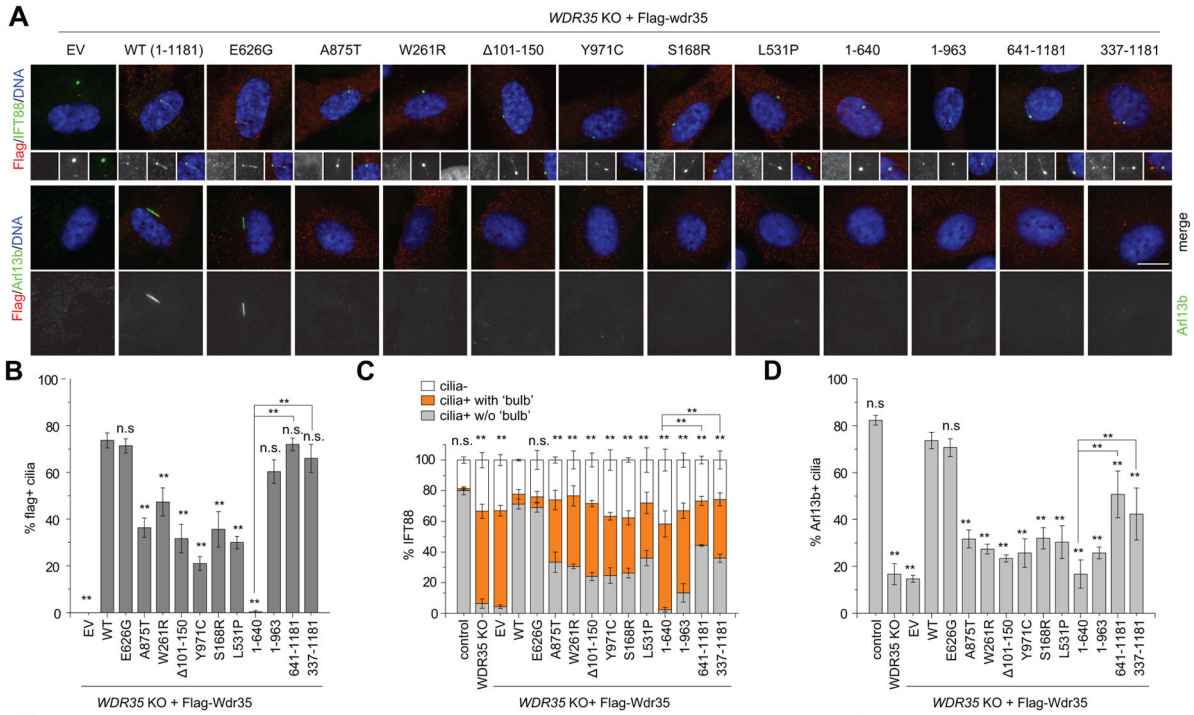

E

Interactions	Minimum domains for robust interactions	COP-I template	Homology-based prediction
Wdr35-IFT122	1-640, 545-800	α-β′ dimer	around 699-750, dimer
Wdr35-Ttc21b	545-1181	α-β, β′-β and α-ε	641-750 and 951-1181
Wdr35-Arl13b	1-200, 545-800	α-cargo and β′-cargo	1-331
Wdr35-INPP5E	1-640, 545-1181	α-cargo and β′-cargo	1-331
Wdr35-IFT43	545-1181, strong interaction	not found	not found
Wdr35-Cep290	1-1181	not found	not found
IFT122-IFT139	domain not analyzed	α-β and β′-β	like Wdr35-Ttc21b
IFT122-Arl13b/INPP5E	domain not analyzed	α-cargo and β′-cargo	like Wdr35-cargo
Ttc21b-Arl13b	domain not analyzed	β-Arf1-membrane	not found
IFT43-INPP5E	weak interaction	not found	not found

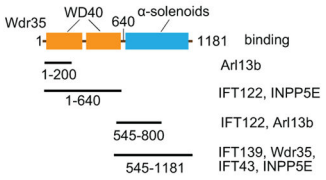

Figure 6. Wdr35-dependent retrograde intraflagellar transport and membrane cargo entry share a common mechanism

(A) *WDR35* KO (#2) cells were rescued by infection with lentiviruses expressing different Flag-tagged Wdr35 constructs. Several disease-related and truncation mutants were analyzed. Representative images of IFT88 and Arl13b are shown. Scale bar, 10 μm. (B–D) Cilia targeting efficiency of Wdr35 constructs (B), IFT88 localization in cilia (C), and percentages of Ar13b+ cilia shown in (A) were quantified. Mutants with the strongest defects in IFT88 transport also exhibit most severe defects in cilium targeting of Arl13b. Asterisks over each bar indicate its difference with *WDR35* KO rescued with WT in (B–D), and asterisks in (C) indicate significance of occurrence of bulbous IFT88. $^{**}P < 0.01$. n.s., not significant. (E) Comparison of computational analysis with mapped Interactions of IFT-As based on IP results. The regions required for COPI complex formation were aligned to Wdr35 regions based on sequence similarity, i.e., homology-based prediction. Numbers indicate the minimum regions in Wdr35 required for robust interactions. (F) Schematic showing the minimal regions in Wdr35 required for various interactions. **See also** Figure S7 and Table S2.

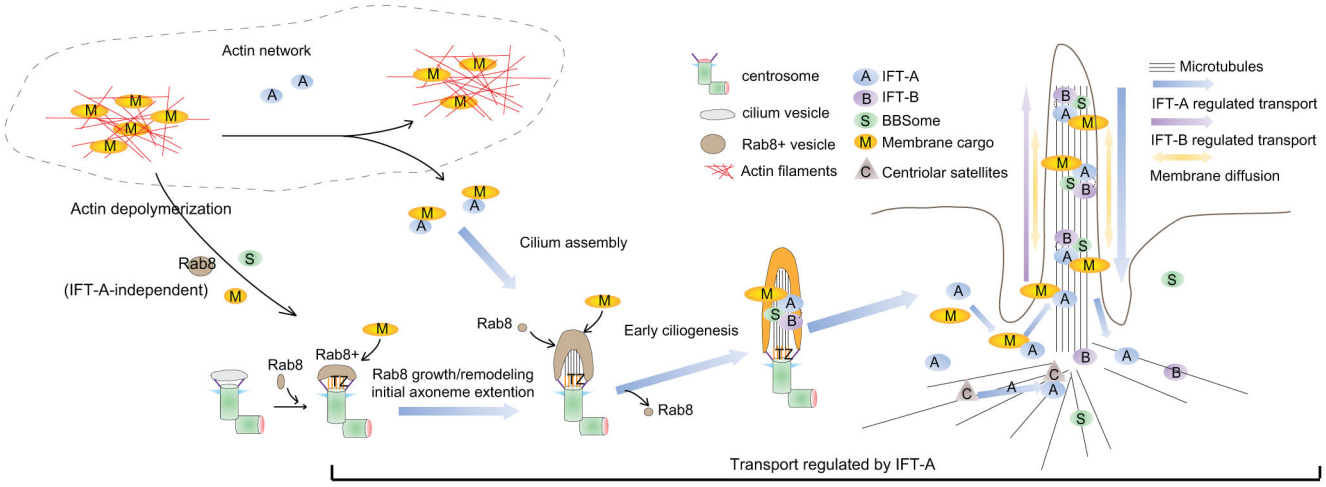

Figure 7. A Model depicting the role of Wdr35-containing IFT-A complex in regulating the cargo transport network during cilium assembly

See text for details.